Microrheology and ROCK Signaling of Human Endothelial Cells Embedded in a 3D Matrix

Porntula Panorchan,* Jerry S. H. Lee,* Thomas P. Kole,* Yiider Tseng,† and Denis Wirtz*‡

*Department of Chemical and Biomolecular Engineering, The Johns Hopkins University, Baltimore, Maryland 21218; †Department of Chemical Engineering, University of Florida, Gainesville, Florida 32611; and ‡Department of Material Science and Engineering, Howard Hughes Medical Institute Graduate Training Program, and Institute for NanoBioTechnology, The Johns Hopkins University, Baltimore, Maryland 21218

ABSTRACT Cell function is profoundly affected by the geometry of the extracellular environment confining the cell. Whether and how cells plated on a two-dimensional matrix or embedded in a three-dimensional (3D) matrix mechanically sense the dimensionality of their environment is mostly unknown, partly because individual cells in an extended matrix are inaccessible to conventional cell-mechanics probes. Here we develop a functional assay based on multiple particle tracking microrheology coupled with ballistic injection of nanoparticles to measure the local intracellular micromechanical properties of individual cells embedded inside a matrix. With our novel assay, we probe the mechanical properties of the cytoplasm of individual human umbilical vein endothelial cells (HUVECs) embedded in a 3D peptide hydrogel in the presence or absence of vascular endothelial growth factor (VEGF). We found that VEGF treatment, which enhances endothelial migration, increases the compliance and reduces the elasticity of the cytoplasm of HUVECs in a matrix. This VEGF-induced softening response of the cytoplasm is abrogated by specific Rho-kinase (ROCK) inhibition. These results establish combined particle-tracking microrheology and ballistic injection as the first method able to probe the micromechanical properties and mechanical response to agonists and/or drug treatments of individual cells inside a matrix. These results suggest that ROCK plays an essential role in the regulation of the intracellular mechanical response to VEGF of endothelial cells in a 3D matrix.

INTRODUCTION

Moving cells from a two-dimensional (2D) culture dish to a more physiological three-dimensional (3D) matrix induces profound changes in cell morphology and function. Fibroblasts grown on a 2D matrix-coated substrate adopt a flattened morphology, display prominent contractile actomyosin stress fibers, and typically move slowly through a multi-step mechanism of polarized extension, substrate binding, and actin-based contraction (1). In contrast, fibroblasts embedded in a matrix adopt a spindle-like morphology, frequently lack stress fibers and discrete focal contacts, and move through integrin-dependent processes that are coupled to matrix reorganization (2). Endothelial cells placed on a matrix layer proliferate to confluence, whereas the same cells sandwiched between two matrix layers can form extended tubular structures that resemble blood vessel capillaries in vivo (3). Mammary gland cells placed on a 2D collagen substratum are flattened and secrete little or no casein. However, when embedded inside a floating collagen matrix, these cells display a characteristic cuboidal-to-columnar epithelial morphology and secrete abundant amounts of casein (4). These are but a few examples that illustrate how normal cell function can be inhibited when cells are plated on a nonphysiological flat substrate (2).

This cell function switch induced by a change of geometry typically involves major actin cytoskeleton remodeling mediated by matrix-integrin-cytoskeleton interactions (5,6). Actin cytoskeleton remodeling is orchestrated by the Rho family of small GTPases (7), of which the best studied are RhoA, Rac1, and Cdc42 (8). In particular, active GTP-bound RhoA can recruit members of the ROCK (ROK/Rho-kinase) family, which phosphorylate cytoskeleton proteins involved in cell contractility, and the ezrin-radixin-moesin family proteins, which link the actin cytoskeleton to the cell membrane (9). ROCK regulates the contractility of actin-myosin contractile fibers by controlling the phosphorylation of myosin light chain kinase (10). However, the answers to the fundamental questions of whether and how ROCK regulates the intracellular mechanical response of cells in a matrix are unknown.

Current cell-mechanics methods cannot measure the mechanical response of individual cells in a 3D matrix (Fig. 1 *A*). Indeed, cells embedded in an extended matrix, although amenable to imaging through confocal microscopy and reflection microscopy (11), are inaccessible to conventional physical probes. These include atomic force microscopy (AFM) (12), glass microneedles (13), membrane-bound magnetic beads (14), micropipette suction (15), and microplate manipulation (16). Although these methods have been useful to probe the mechanical properties of suspension and adherent cells, they all require a direct contact with the cell surface, which makes them unsuitable to probe the mechanics of cells that are embedded inside a 3D matrix.

We have recently introduced the method of intracellular microrheology (ICM) (17), which probes the micromechanical properties of the cytoplasm of cells adherent to a flat 2D

Submitted March 10, 2006, and accepted for publication July 18, 2006.

Address reprint requests to Denis Wirtz, Dept. of Chemical and Biomolecular Engineering, The Johns Hopkins University, 3400 N. Charles St., Baltimore, Maryland 21218. Tel.: 410-516-7006; Fax: 410-516-5510; E-mail: wirtz@jhu.edu.

0006-3495/06/11/3499/09 $2.00

doi: 10.1529/biophysj.106.084988

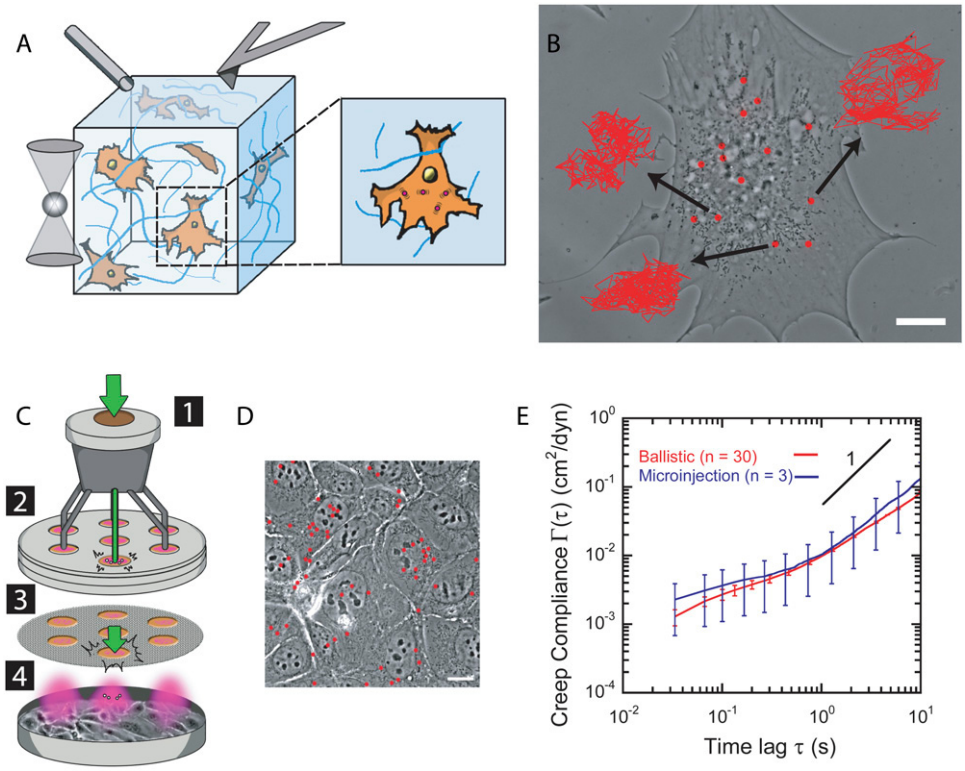

FIGURE 1 Ballistic injection of nanoparticles for particle tracking in live cells embedded in a 3D matrix. (*A*) Schematic of cells embedded in an extended 3D matrix. These cells are readily amenable to imaging but are not accessible to physical probes that require direct contact with the cell, such as AFM (*upper right*), optical tweezers (*middle left*), and calibrated microneedles (*upper right*). We developed a microscopy assay based on high-resolution tracking of nanoparticles ballistically bombarded into the cytoplasm of live cells to probe the micro mechanical properties of single endothelial cells embedded in a 3D matrix (*right*). (*B*) Phase-contrast micrograph of a Swiss 3T3 fibroblast overlaid with a fluorescent micrograph of 100-nm-diameter nanoparticles that were ballistically injected into the cytoplasm. (*C*) Schematic of the ballistic nanoparticle delivery system used in the experiments. (*1*) Helium gas is accelerated through a gas chamber through a rupture disk, which (*2*) impacts into macrocarrier disks coated with fluorescent nanoparticles, and (*3*) forces them to crash into a stopping screen. (*4*) The momentum of the macrocarrier is transferred to the nanoparticles, which penetrate the target cells. (*D*) Culture of Swiss 3T3 fibroblasts with ballistically injected fluorescent nanoparticles. The size of the nanoparticles in panels *B* and *D* was enlarged to aid visualization. (*E*) Comparison between the mean creep compliance (mechanical deformability of the cytoplasm) computed from the displacements of nanoparticles microinjected (*blue line*) ($n = 3$ cells) and ballistically bombarded (*red line*) ($n = 30$ cells) into the cytoplasm of Swiss 3T3 fibroblasts. High values of compliance indicate a soft material; low values of compliance indicate a stiff material. Values are mean ± SE.

substrate. In this method, the extent of the random movements of submicron particles microinjected into the cytoplasm measures its local viscoelasticity. Like other cell mechanics methods, the method of microrheology in its current form cannot be utilized to probe cells embedded in a matrix: the few microinjected cells that are subsequently detached from their substrate cannot readily be found once embedded in an extended matrix.

Here we introduce a new method to probe for the first time the micromechanical properties of single cells embedded inside an extended 3D matrix. Fluorescent nanoparticles are ballistically bombarded into the cytoplasm of cells plated on a flat culture dish. These injected cells are then detached from the dish and subsequently embedded in the matrix. The spontaneous movements of the nanoparticles are then tracked with high spatial and temporal resolutions using time-lapsed fluorescence microscopy. The random trajectories of the nanoparticles are analyzed to ultimately compute the viscoelastic properties of the cytoplasm of individual cells embedded in a matrix. To establish a proof of principle, we use our new assay to probe the viscoelastic properties of the cytoplasm of human umbilical vein endothelial cells (HUVECs) embedded in a 3D peptide hydrogel matrix. We further test the versatility of our assay by probing the mechanical response of HUVECs in the matrix to vascular endothelial growth factor (VEGF). To obtain more nutrient and oxygen during tumor invasion and proliferation, tumor cells release VEGF to promote endothelial migration and angiogenesis. Here we use combined particle-tracking microrheology and ballistic injection to investigate the mechanical effects of VEGF on endothelial cell migration in a matrix and study the role of ROCK on the regulation of this mechanical response to VEGF.

MATERIALS AND METHODS

Cell culture

HUVEC-C (ATCC, Manassas, VA) were cultured in Ham's F12K medium with 2 mM L-glutamine adjusted to contain 1.5 g/liter sodium bicarbonate and supplemented with 0.1 mg/ml heparin, 0.05 mg/ml of endothelial cell growth supplement (ECGS), and 10% fetal bovine serum (HUVECs complete growth medium). Swiss 3T3 fibroblasts (ATCC, Manassas, VA) were cultured in complete DMEM (c-DMEM; Dulbecco's Modified Eagle Medium supplemented with 10% bovine calf serum, ATCC). Cell cultures were maintained at 37°C in a humidified, 5% CO_2 environment. All measurements were performed in an incubator mounted on an inverted microscope maintained at 37°C with 5% CO_2 and humidity.

Peptide hydrogels

Cells were seeded in puramatrix peptide hydrogels (BD Biosciences, San Jose, CA). HUVECs were resuspended in 10% sucrose solution and diluted

1:1 with peptide solution to obtain a final peptide concentration of 0.5% and a cell density of 1×10^6 cells/ml. The suspension was quickly mixed and pipetted into a 500-μl well casing. The well was then filled with growth medium to initiate self-assembly of the peptide gel into a supporting 3D scaffold. The 3D cell culture was maintained at 37°C with 5% CO_2 overnight before experiments.

VEGF treatment and ROCK inhibition

VEGF (NCI, Rockville, MD) was prepared as a stock solution of 1 μg/ml in sterile PBS containing 0.1% BSA (w/v). Bombarded cells were used in the following experiments: 1), control experiments: bombarded cells were seeded overnight before microrheological analysis (see next paragraph); 2), VEGF treatment: bombarded cells were treated with HUVECs complete growth medium supplemented with 4 ng/ml VEGF for 24 h before microrheological analysis; and 3), VEGF and Y-27632 combination treatment: bombarded cells were treated with HUVECs complete growth medium supplemented with 4 ng/ml VEGF for 24 h and 30 μM Y-27632 for 30 min before data collection.

Ballistic injection and intracellular rheology from particle tracking

To probe the local mechanical properties of the cytoplasm of living cells embedded in a 3D matrix, we introduced a new assay, modified from the method of ICM (18,19). Fluorescent polystyrene nanoparticles 100 nm in diameter were introduced into the cytoplasm of living cell using a ballistic gun (Bio-Rad, Hercules, CA). In this method of injection, helium is accelerated through a gas chamber, which forces a macrocarrier disk coated with the fluorescent nanoparticles to crash into a stopping screen. The momentum of the macrocarrier is transferred to the nanoparticles, which penetrate the target cells. Problems could arise when nanoparticles that do not directly penetrate the cytoplasm on impact and are engulfed by the cell through endocytosis and may then undergo microtubule-mediated directed motion. We avoided this possible pitfall by thoroughly and repeatedly washing the cells with fresh medium right after ballistic bombardment. We note that we never observed directed motion of the nanoparticles. Of the cells exposed to ballistic injection, 30–40% survived. The dead cells were washed away; the surviving cells were embedded in hydrogels for the experiments. After ballistic injection, cells were embedded in a matrix (see above) and incubated overnight at 37°C with 5% CO_2/air.

The local micromechanical properties of the cytoplasm of cells embedded in a matrix were measured by tracking the spontaneous motion of the ballistically injected nanoparticles. Cells were placed in an incubator mounted on an inverted microscope maintained at 37°C with 5% CO_2/air. Capture of movies of fluctuating nanoparticles in the cytoplasm of cells and computation of the mean-squared displacements (MSDs) of each nanoparticle in the plane of focus of the microscope (expressed in μm^2)

$$\langle \Delta r^2(\tau) \rangle = \langle [x(t+\tau) - x(t)]^2 \rangle + \langle [y(t+\tau) - y(t)]^2 \rangle$$

were executed using multiple-particle-tracking software, as described (18). Here, $x(t)$, $y(t)$ are the 2D time-dependent coordinates of a nanoparticle in the x and y directions of the plane of focus; t is the elapsed time; τ is the time lag; and the brackets represent time averaging. The value of the MSD of a nanoparticle at a given time lag τ indicates how far it has traveled during that time. Detailed studies that examine the effects of size and surface chemistry, as well as the mode of delivery of the nanoparticles on the movements in the cytoplasm of live cells can be found in Kole et al. (18). The time of capture of each movie (20 s) is much shorter than the characteristic time scales of cell migration. The majority of the nanoparticles remained in the field of view during the time of movie capture.

We found that the time-averaged displacements of the nanoparticles in the x and y directions were identical, i.e., $\langle [x(t+\tau) - x(t)]^2 \rangle = \langle [y(t+\tau) - y(t)]^2 \rangle$. Therefore, we assumed that the out-of-plane displacements (in the z direction) of the nanoparticles were equal to those in the x and y directions. The two-dimensional MSD of each probe nanoparticle is directly related to the local creep compliance of the cytoplasm (20), $\Gamma(\tau)$, as

$$\Gamma(\tau) = \frac{3\pi a}{2k_B T} \langle \Delta r^2(\tau) \rangle.$$

The creep compliance Γ (expressed in $cm^2/dyn = 10\ Pa^{-1}$, which are units of inverse pressure or modulus) describes the local deformation of the cytoplasm induced by the fluctuating forces acting on the surface of the nanoparticles and generated by their spontaneous displacements.

All rheological information about the cytoplasm is contained in the creep compliance as a function of time lag τ. However, traditional methods of cell rheology typically measure viscoelastic moduli. Therefore, we also calculated viscoelastic moduli from creep compliance measurements. The frequency-dependent viscoelastic parameters of the cytoplasm (expressed in $dyn/cm^2 = 0.1$ Pa), $G'(\omega)$ and $G''(\omega)$, were computed straightforwardly from the MSD, as described previously by Kole et al. (18). The elastic modulus, G', and viscous modulus, G'', describe the propensity of a complex fluid to store energy and flow, respectively. An entangled filamentous network, such as a reconstituted F-actin network (21–24) or the cytoplasm of endothelial cells (this work), typically behaves like an elastic solid at high rates of shear (high frequencies ω), when filaments do not have the time to relax during shear, and like a liquid at low rates of shear. The mean shear viscosity of the cytoplasm (expressed in Poise = 1 Pa·s) was approximated as the product of the mean relaxation time (inverse of the frequency for which $G'(\omega) = G''(\omega)$) and the mean plateau value of the elastic modulus of the cytoplasm (value of G' for which G' is approximately constant).

Unless indicated, we report the mean creep compliance and mean viscoelastic moduli, i.e., the compliance and viscoelastic moduli, of the cytoplasm averaged over all tracked nanoparticles and all probed cells in a given condition.

Microscopy

After each experiment, cells were fixed and stained to examine actin filament organization. Cells were fixed in 2.5% paraformaldehyde in phosphate-buffered saline (Life Technologies, Gaithersburg, MD) and permeabilized in 0.1% Triton X-100 (Sigma) in PBS. Cells were blocked in 10% FBS for 30 min at room temperature and labeled with Alexa 488 phalloidin (Molecular Probes) at 1:40 dilution for 1 h at room temperature. Specimens were mounted in Prolong Gold antifade (Invitrogen) to reduce photobleaching. Cell morphology and fluorescently labeled cells were examined by phase-contrast and fluorescence microscopy, respectively. Images were acquired using a Nikon Eclipse TE2000-E inverted microscope equipped with a 60×, oil-immersion objective (N.A. 1.4) and a Cascade 1k camera (Roper Scientific, Tucson, AZ) controlled by the Metaview software (Universal Imaging).

Statistical analysis

Ballistic injection delivers nanoparticles to an entire 100-mm tissue culture dish, which contains on the order of 10^6 cells. With 10–20% nanoparticle penetration success rate, each ballistic injection yielded an order of 10^4–10^5 nanoparticle-loaded cells. Manual microinjection may yield 10–30 nanoparticle-loaded cells. When used in conjunction with particle tracking, microinjection yielded a typical population size of only three to five cells. Therefore, ballistic injection provides a 1000-fold increase in cells available for data acquisition. Using a population size of 30 cells, each cell with ~15–20 nanoparticles, limited the standard error of the mean (SE) to 15%. With this population size, we found that the data follow a well-defined Gaussian distribution, which allows for robust application of statistical analysis. Data are expressed as the mean ± SE, unless otherwise stated. Statistical significance between the differences of creep compliances from different conditions were determined by paired Student's t-test. Values of $P < 0.01$ were considered to be statistically significant.

RESULTS

Ballistic injection and intracellular rheology from multiple particle tracking

ICM, which couples microinjection of submicron nanoparticles with their high-resolution tracking in the cytoplasm, has proved to be an extremely powerful method to probe the rheological properties of live cells (17–19,25,26) (Fig. 1 *A*). However, ICM presents the drawback of requiring the manual microinjection of nanoparticles, which is tedious and time consuming. Direct delivery of nanoparticles into the cytoplasm is required to circumvent endocytosis of the nanoparticles and, therefore, avoid their noncontrolled, directed motion mediated by motor proteins. Moreover, ICM can probe only a relatively small number of cells for a reasonable time of injection. This problem prevents the use of ICM for cells in complex geometries, such as cells embedded in an extended matrix studied here. This is because, once detached from their substratum and being placed inside a 3D matrix, the few injected cells cannot be found.

To preserve the advantage of ICM of measuring directly the mechanical properties of the cytoplasm and render ICM high throughput, we introduce ballistic injection. A biolistic particle delivery system is used to deliver 100nm-diameter polystyrene fluorescent nanoparticles to cultured cells. Helium gas at a pressure of 2200 psi is used to force a macrocarrier disk coated with fluorescent nanoparticles to collide into a stopping screen, which delivers the nanoparticles into target cells (Fig. 1 *C*). The gas pressure was adjusted to maximize the number of injected cells while minimizing cell death. Ballistic injection increased ~1000-fold the number of cells available for data acquisition compared to manual injection (Fig. 1, *B–D*).

To validate ballistic injection and ensure that it did not affect the evaluation of intracellular mechanics parameters, we compared the mean viscosity and mean elasticity of the cytoplasm of Swiss 3T3 fibroblasts plated on glass (Fig. 1 *B*) by tracking nanoparticles that were either microinjected or ballistically bombarded into the cells. We used Swiss 3T3 fibroblasts because these cells have been characterized extensively using ICM (17–19,25). We compared directly the mean viscoelastic properties of the cells from conventional ICM to those obtained from using our new assay: ballistic intracellular nanorheology (BIN). Here the mean creep compliance is the deformability of the cytoplasm averaged over all tracked nanoparticles and all probed cells. We found quantitative agreement between the mean creep compliance following both modes of injection, although many more cells were probed using ballistic injection (Fig. 1 *E*).

The creep compliance describes the local deformation of the cytoplasmic region surrounding the nanoparticles induced by their spontaneous displacements powered by thermal energy. The creep compliance grows with time, $\Gamma(\tau) \sim \tau$ if the cytoplasm behaves as a viscous liquid and is mostly constant if the cytoplasm behaves as an elastic solid, $\Gamma(\tau) \sim$ constant. Here the movements of the nanoparticles were subdiffusive, and the creep compliance had a power-law behavior with a time lag dependence intermediate between 0 and 1 (Fig. 1 *E*), i.e., $\Gamma(\tau) \sim \tau^{\alpha}$, where $0 < \alpha < 1$. This result indicates that the cytoplasm behaved as a viscoelastic material. It also indicates than nanoparticles ballistically injected into the cells (which were incubated overnight) did not undergo directed motion. For nanoparticles undergoing directed motion, their movements would be superdiffusive, and $\Gamma(\tau) \sim \tau^{\alpha}$, where $\alpha > 1$, which was never observed.

Together these results imply that ballistic injection does not introduce artifacts in the evaluation of intracellular mechanics from MSD measurements and that measurements of intracellular rheology by ICM and BIN agree quantitatively.

Probing the rheology of single endothelial cells embedded inside a matrix

To demonstrate the use of BIN to probe the micromechanics of single cells inside a matrix, we probed the intracellular mechanical properties of single HUVECs embedded in a peptide hydrogel. HUVECs were plated on a culture dish, ballistically injected with 100-nm-diameter fluorescent polystyrene nanoparticles, detached from their substrate (through trypsin treatment followed by washing), and embedded in a 3D peptide (puramatrix) hydrogel.

Single HUVECs embedded at low density in the matrix displayed a dramatically different morphology from that of HUVECs plated at low density on a layer of the same matrix (27,28). Cells plated on the matrix displayed a wide lamella and extensive stress fibers that spanned the length of the cell (data not shown). Cells embedded in the matrix showed extensive dendritic protrusions, few organized actin filament bundles, and an actin-rich rim at the cell periphery (Fig. 2 *A*).

By tracking the random displacements of nanoparticles ballistically injected in the cytoplasm of HUVECs (Fig. 2 *A*), we studied the intracellular mechanics of these cells in a 3D matrix. The MSDs of the nanoparticles were mathematically transformed into creep compliance and viscoelastic moduli following standard methods (18) (Fig. 2, *B* and *C*). Here we document both the compliance and viscoelastic moduli of the cytoplasm because the local compliance is directly proportional to the MSD of the probe nanoparticles (and therefore requires no mathematical transformation), although moduli can be compared to values obtained with other viscoelastic materials or reconstituted cytoskeletal filament networks. The elastic modulus, G', and viscous modulus, G'', describe the propensity of the cytoplasm to store energy when deformed by mechanical stresses (caused by the random movements of the probe nanoparticles) and to flow, respectively.

Similarly to fibroblast on glass, HUVECs in a 3D matrix showed both significant elasticity and viscosity (Fig. 2 *C*). The cytoplasm of these cells was more viscous than elastic ($G'' > G'$) at low rates of deformations ($\omega < 0.4$ Hz), which from a rheological standpoint corresponds to a viscoelastic liquid. The cytoplasm of these cells was more elastic than

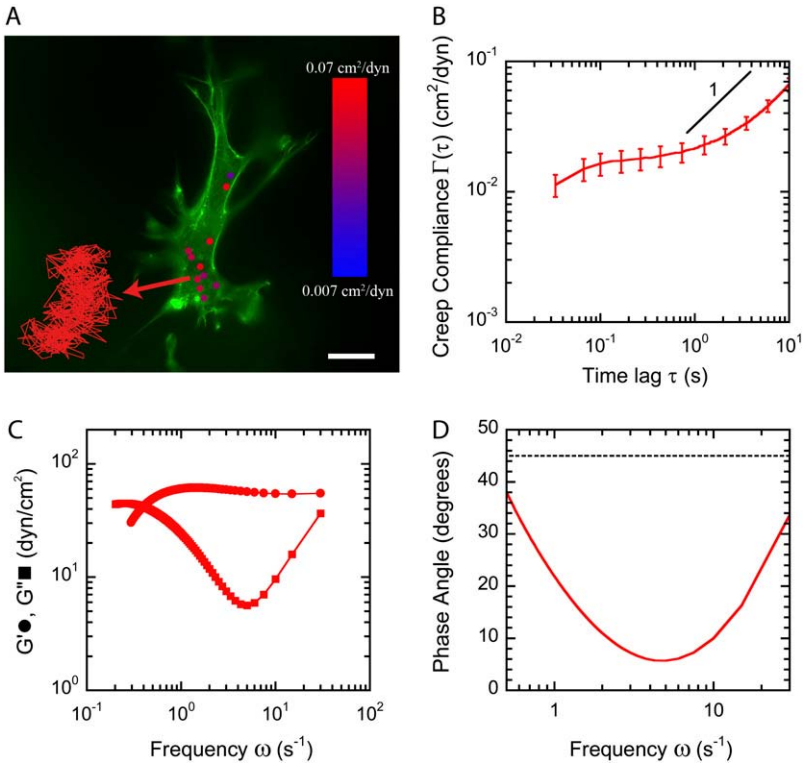

FIGURE 2 Local micromechanics of the cytoplasm of HUVECs embedded in a matrix. (*A*) Fluorescent micrograph of the actin filament network in a HUVEC embedded in the 3D peptide (puramatrix) hydrogel, overlaid with a fluorescent micrograph of nanoparticles embedded in the cytoplasm. Each nanoparticle was color-coded according to the value of the local deformability (evaluated at a time scale of 0.1 s). The size of the nanoparticles was increased to aid visual presentation. Blue denotes the least compliant (stiffest) regions of the cytoplasm; red denotes the most compliant (softest) regions of the cytoplasm. Actin filaments were visualized with Alexa 488 phalloidin. Bar, 20 μm. A typical trajectory of a nanoparticle in the cytoplasm of a HUVEC is also shown. (*B*) Mean cellular deformability (compliance) ($n = 33$ cells; 244 nanoparticles) of HUVECs in a 3D matrix. Values are mean ± SE. The indicator slope of 1 indicates that the mean cytoplasmic compliance grows less rapidly than time lag. (*C*) Mean frequency-dependent viscous and elastic moduli, $G'(\omega)$ (*circles*) and $G''(\omega)$ (*squares*), obtained by mathematical transformation of the mean cellular compliance shown in panel *B*. (*D*) Phase angle, $\delta(\omega) = \tan^{-1}[G''(\omega)/G'(\omega)]$, which quantifies the viscous versus elastic nature of the cytoplasm. The phase angle was computed from G' and G'' data in panel *C*. A phase angle of 0° would correspond to the rheological response of an elastic solid; a phase angle of 90° would correspond to the rheological response of a viscous liquid such as water. Here, the phase angle is lower than 45° (indicated by the *horizontal line*); i.e., the cytoplasm behaves as a viscoelastic solid over a wide range of rates of deformation ω.

viscous ($G'' < G'$) at high rates of deformation (Fig. 2 *C*), which corresponds to a viscoelastic solid.

The viscoelastic nature of the cytoplasm of HUVECs in a 3D matrix can be quantified by the phase angle, $\delta = \tan^{-1}(G''/G')$ (Fig. 2 *D*). The phase angle describes the delay between imposed (input) deformation of the cytoplasm and resulting (output) mechanical stress induced in the cytoplasm by the random movements of the nanoparticles. This delay is maximum for a viscous liquid ($\delta = 90°$) and minimum for an elastic solid ($\delta = 0°$). Here, the phase angle was minimum at an intermediate rate of shear (frequency ω) of ~4 Hz (Fig. 2 *D*), which corresponded to the frequency where G'' is minimum while G' adopts a plateau value (Fig. 2 *C*). The phase angle reincreased toward a value of 45° at low and high frequencies (Fig. 2 *D*), for which G'' became closer to G' (Fig. 2 *C*). Reconstituted cross-linked actin filament suspensions in vitro display a similar complex viscoelastic behavior (21,29).

The plateau value of G' of HUVECs embedded in a hydrogel was ~60 dyn/cm^2; the mean shear viscosity of their cytoplasm was 13 Poise. By comparison, the viscosities of glycerol (no added water) and corn syrup are ~10 Poise and ~25 Poise, respectively.

Probing the rheological response to VEGF of single endothelial cells embedded in a matrix

VEGF enhances the angiogenic migration of endothelial cells (30,31) and activates signaling pathways that regulate actin assembly (32) (Fig. 3, *A* and *B*). We found that VEGF increased the compliance and decreased the elasticity of the cytoplasm of HUVECs placed inside the 3D peptide matrix (Fig. 3, *C* and *D*).

To begin to elucidate the molecular mechanisms by which a single HUVEC in a 3D matrix responds to VEGF stimulation, we targeted ROCK, which is known to regulate actin organization in HUVECs following VEGF stimulation (33) (Fig. 4 *A*). The cells were subjected to VEGF and simultaneously treated with specific ROCK inhibitor Y-27632 (34). We found that Y-27632 treatment abrogated VEGF-induced softening of HUVECs inside a matrix (Fig. 4, *B* and *C*). Together these results suggest that ROCK plays an essential role in the regulation of the intracellular mechanical response to VEGF of endothelial cells in a 3D matrix.

DISCUSSION

We introduce a new protocol that combines the well-established method of ICM with the newly developed ballistic cell-bombarding method to probe the rheology of single cells placed in the more physiological 3D environment of a matrix. Ballistic injection followed by high-resolution tracking of the probe nanoparticles in the cytoplasm allows us to probe for the first time the micromechanical properties of the cytoskeleton of single cells embedded inside a matrix. This method does not require direct contact between cell and physical probe. It

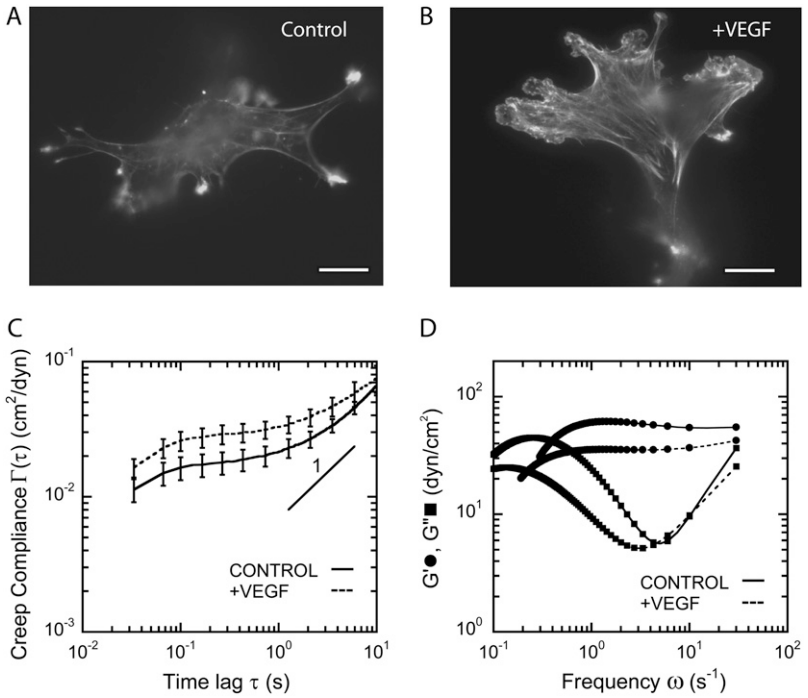

FIGURE 3 Mechanical response of HUVECs embedded in a matrix to VEGF. (*A* and *B*) Fluorescent micrographs of actin filaments of HUVECs in a 3D matrix (*A*) in the absence of VEGF and (*B*) in the presence of VEGF. Actin filaments were visualized with Alexa 488 phalloidin. Bar, 20 μm. (*C*) Mean creep compliances of the cytoplasm of HUVECs in a 3D matrix in the absence of VEGF (*bottom*, *solid line*) ($n = 33$ cells; 244 nanoparticles) and presence of VEGF (*top*, *dashed line*) ($n = 10$ cells; 50 nanoparticles). (*D*) Mean viscoelastic moduli G' (*circles*) and G'' (*squares*) of HUVECs in a 3D matrix in the absence of VEGF (*solid line*) and the presence of VEGF (*dashed line*). Compliances in panel *C* are mean $\pm$ SE. Moduli in panel *D* were calculated using the data in panel *C*. The differences in compliances (panel *C*) and viscoelastic moduli (panel *D*) between the control HUVECs and the VEGF-treated HUVECs were significant (P values over the entire time lag time/frequency ranges <0.05).

complements traditional assays that measure global mechanical effects on matrices containing contractile cells (35–37). Ballistic injection also allows us to probe a much larger pool of cells than conventional microinjection, transforming the method of ICM into a high-throughput biophysical method, which we name ballistic intracellular nanorheology (BIN).

Advantages of BIN to probe cell micromechanics

For proper computation of the rheological parameters from MSD measurements, the nanoparticles used for cell nanorheology measurements cannot interact with subcellular structures or be actively transported (17). Such interactions or directed transport would uncontrollably change the MSD profiles and therefore would affect artificially the calculation of viscoelastic properties of the cytoplasm from MSD measurements. Therefore, the nanoparticles used in cell nanorheology cannot be transferred to the cytoplasm via endocytosis by simply being placed on the surface of the cells (17). Nanoparticles delivered to the cytoplasm in this manner are enveloped in large vesicles, which are themselves connected to motor proteins (dynein) that shuttle the vesicles toward the nucleus (38). In this case, there is no intimate contact between the nanoparticles and the intracellular milieu to be probed, and the nanoparticles undergo directed motion. Use of ballistic injection allows the endocytic pathway to be circumvented.

BIN offers new advantages compared to conventional ICM (17–19). These include:

1. In a single ballistic injection, the number of injected cells amenable to measurements increases by 1000-fold compared to traditional microinjection.
2. Microinjection of cells can be inconsistent because of the invasive nature of injection and the mechanical trauma to the cells that ensues. With ballistic injection, every cell is injected similarly, thus decreasing cell-to-cell variations in the measurements of cytoplasmic viscoelasticity sometimes found after microinjection.
3. With a large population of injected cells, BIN allows us to probe single-cell mechanics in complex geometries and in more physiological situations. These include probing the mechanical response of the cytoskeleton in cells subjected to shear flows (39), probing the differential mechanical response of cancer cells at the rear and the edge of a wound (J. S. H. Lee, P. Panorchan, and D. Wirtz, unpublished data), and probing cells embedded inside a 3D matrix, as demonstrated in this article.
4. With a large sample size per condition (number of probed cells $\sim$30), our results become more precise. Microinjection leads to small sample size (number of probed cells $\sim$5), which is subject to cell-to-cell variations and more prone to random experimental errors. BIN provides more precise and consistent values for global and local viscoelastic properties.

In addition, BIN offers the same advantages as ICM:

1. BIN can measure directly the mechanical properties of the cytoplasm. Most current single-cell mechanics methods require a direct contact between the cell surface and a physical probe. Therefore, these methods cannot distinguish the contribution of the plasma membrane from the contributions of the nucleus and cytoskeleton without making assumptions. In contrast, BIN measures the mechanical properties of the cytoplasm directly.

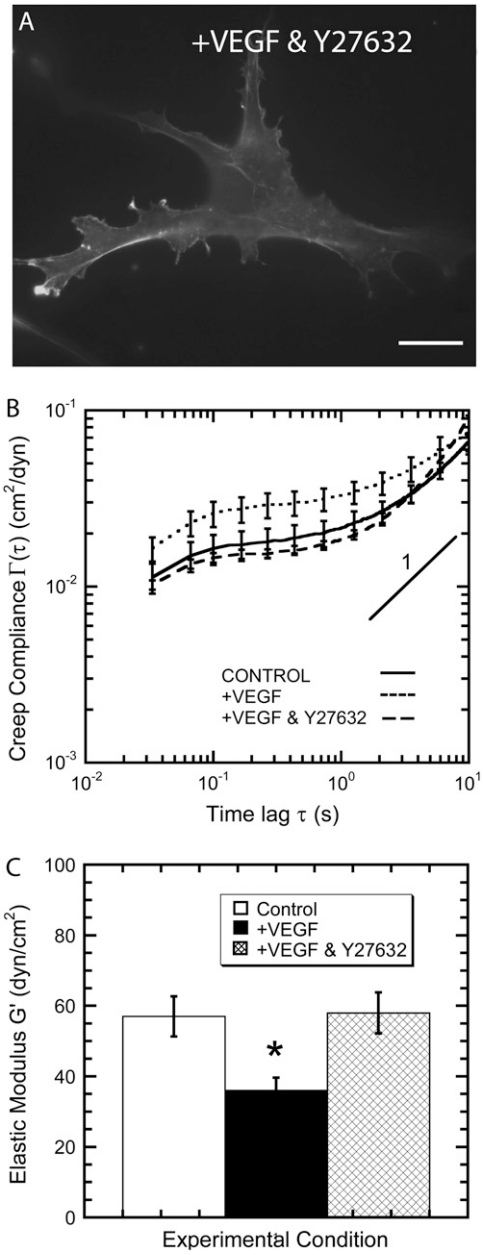

FIGURE 4 ROCK regulates the mechanical response of HUVECs embedded in a matrix to VEGF. (*A*) Fluorescent micrograph of the actin filament network in a HUVEC in a 3D matrix in the presence of VEGF and specific ROCK inhibitor Y-27632. Actin filaments were visualized with Alexa 488 phalloidin. Bar, 20 μm. (*B*) Mean creep compliance (deformability) of the cytoplasm of control HUVECs (*middle*, *solid line*), VEGF-treated HUVECs (*top*, *short-dashed line*), and HUVECs treated with VEGF and Y27632 (*bottom*, *long-dashed line*) ($n = 21$ cells; 119 nanoparticles). (*C*) Mean elastic modulus of the cytoplasm of control (*first column*, *white*), VEGF-treated (*second column*, *black*), and HUVECs treated with VEGF and Y27632 (*third column*, *cross-hatched*). The elastic modulus, G', was evaluated at a frequency of 1 Hz. The elasticity of the cytoplasm of VEGF-treated cells was significantly lower than that of control cells ($P < 0.01$; indicated by an *asterisk*); the elasticity of the cytoplasm of cells treated with both VEGF and Y-27632 was not significantly different from that of control cells ($P > 0.5$). Values in panels *B* and *C* are mean ± SE.

2. BIN measures shear-rate dependent viscoelastic moduli. This is particularly crucial for the cytoskeleton, which behaves like a liquid at long time scales (or low rates of shear) and like an elastic solid at short time scales (or high rates of shear).
3. By tracking multiple nanoparticles simultaneously, BIN can measure the micromechanical response to stimuli or drug treatments of various compartments of the cells simultaneously (19). By using video-based multiple particle tracking instead of laser-deflection particle tracking (40), hundreds of nanoparticles embedded in the body of cells can be tracked at the same time.
4. BIN rheological measurements are absolute and compare favorably with traditional rheometric measurements on standard fluids of known viscosity and elasticity (20,41). This is not the case of single-cell approaches that require a direct contact between the cell surface and the probe.
5. BIN measures elasticity and viscosity. Most approaches cannot directly distinguish the elastic response from the viscous response of a cell.

The method of particle-tracking microrheology (41–43), on which ICM and BIN are based, has been tested against standard materials of known viscosity and elasticity. In particular, the viscoelastic moduli G' and G'' of actin filament solutions measured by particle-tracking microrheology and measured using a traditional cone-and-plate rheometer are close (20). This suggests that the viscoelastic moduli measured by BIN do reflect faithfully the true viscoelastic properties of the cytoplasm. Moreover, the values of elasticity for reconstituted actin filament networks containing cross-linking/bundling proteins, such as filamin, α-actinin, or fascin (21,44), are relatively similar to those measured in live cells. However, they are significantly lower than the values of elasticity measured by other methods, such as AFM and glass microneedles (45–47), which probe cell mechanics via physical contact with the plasma membrane and therefore measure the combined responses of the plasma membrane, the cytoplasm, and the nucleus. Together, these observations suggest that the large difference in cell elasticity measured by these methods and by ICM/BIN may be caused by mechanical coupling between the cytoskeleton and the plasma membrane or by the nucleus, which is much stiffer than the cytoplasm (25,48) and is physically connected to the cytoskeleton (49).

ROCK mediates VEGF-induced cytoplasmic softening in HUVECs

It has long been speculated that the dramatic differences in morphology and cytoskeleton organization displayed by cells plated on a substrate and cells in a matrix would elicit differences in the rheological properties of the cytoskeleton to accommodate these changes (35,50). The absence of non-invasive biophysical methods that could measure intracellular viscoelastic parameters of cells embedded in a matrix has

prevented a direct test of that hypothesis. Our results provide direct experimental evidence that cells can adopt dramatically different mechanical properties to adapt to their more physiological 3D matrix environment.

It is important to note that the actin cytoskeleton rearrangements observed by fluorescence microscopy do not always correlate with changes in cytoplasmic rheology. For instance, serum-starved cells subjected to lysophosphatidic acid (LPA) display a dramatic burst in actin polymerization and a rapid and sustained ROCK-mediated contractility (51,52). However, careful microrheological measurements show that cytoplasmic elasticity and viscosity grow and decay rapidly, tracking the rise and decrease of Rho activation, not the (continuous) contractility, observed through fluorescence microscopy, of actin stress fibers terminated by focal adhesions (18). This may be partly a result of the limited resolution and contrast of fluorescence microscopy, which cannot readily detect the presence of a dense actin meshwork between stress fibers (53). This indicates that the absence of organized stress fibers and focal adhesions in cells in a matrix did not a priori signify a softer cytoplasm for these cells. This underlies the requirement for a functional assay that complements the fluorescence microscopy of cytoskeleton structures.

Angiogenesis refers to the process by which new blood vessels are formed within the body. To obtain more nutrients and oxygen during tumor invasion and proliferation, tumor cells release VEGF to promote endothelial migration and angiogenesis. VEGF promotes the formation of highly dynamic protrusions and actin-rich ruffles at the periphery of cells in a 3D matrix and enhances cell migration, as demonstrated by Boyden-chamber and transwell assays (54,55). VEGF also enhances in vitro angiogenesis processes in which endothelial cells are sandwiched between two matrix layers (33). These results together with our findings suggest that VEGF-induced cell motility in a matrix proceeds through the development of highly dynamic lamellipodia protrusions pushing within the cell body against a highly viscous cytoskeleton, whereas for cells in 2D, it proceeds through propulsion against a more elastic cytoskeleton architecture. This is qualitatively supported by recent in vivo visualization of ameba-like migration of metastatic cells in 3D tissues (56).

VEGF-induced endothelial migration is completely abrogated, and VEGF-induced capillary tube formation is greatly reduced, by ROCK inhibition with Y-27632 (33), which also eliminates all VEGF-induced intracellular mechanics changes. To eliminate blood supply to tumors, cancer therapies have targeted the inhibition of angiogenesis. Y-27632 is being tested in patients to eliminate angiogenic migration of endothelial cells.

The biophysical approach developed here establishes a framework to analyze functionally the cytoskeleton rearrangements that occur in cells in a 3D matrix subjected to biochemical stimuli (growth factors, matrix composition, drugs, etc.) or biophysical stimuli (matrix density and stiffness, local forces, etc.). We have identified ROCK as a regulator of cytoplasmic stiffness in endothelial cells embedded in a matrix and subjected to VEGF. The functional assay developed here can now be used to help identify regulators of cell mechanics upstream of RhoA and ROCK. The combination of ballistic injection of nanoparticles and particle-tracking microrheology can also enable the investigation of the mechanical response of endothelial cells subjected to hemodynamic flows (39,57), another situation in which cells cannot be probed using classical cell-mechanics methods because they require a direct contact between cell and probe.

This work was funded by grants from the National Aeronautics and Space Administration (NAG9-1563) and the National Institutes of Health (GM075305 and CA101135) as well as by a graduate training grant from the Howard Hughes Medical Institute.

REFERENCES

1. Nobes, C. D., and A. Hall. 1999. Rho GTPases control polarity, protrusion, and adhesion during cell movement. *J. Cell Biol.* 144:1235–1244.
2. Walpita, D., and E. Hay. 2002. Studying actin-dependent processes in tissue culture. *Nat. Rev. Mol. Cell Biol.* 3:137–141.
3. Folkman, J., and C. Haudenschild. 1980. Angiogenesis in vitro. *Nature.* 288:551–556.
4. Streuli, C. H., N. Bailey, and M. J. Bissell. 1991. Control of mammary epithelial differentiation: basement membrane induces tissue-specific gene expression in the absence of cell-cell interaction and morphological polarity. *J. Cell Biol.* 115:1383–1395.
5. Cukierman, E., R. Pankov, and K. M. Yamada. 2002. Cell interactions with three-dimensional matrices. *Curr. Opin. Cell Biol.* 14:633–639.
6. Cukierman, E., R. Pankov, D. R. Stevens, and K. M. Yamada. 2001. Taking cell-matrix adhesions to the third dimension. *Science.* 294: 1708–1712.
7. Hall, A. 1998. Rho GTPases and the actin cytoskeleton. *Science.* 279: 509–514.
8. Banyard, J., B. Anand-Apte, M. Symons, and B. R. Zetter. 2000. Motility and invasion are differentially modulated by Rho family GTPases. *Oncogene.* 19:580–591.
9. Bar-Sagi, D., and A. Hall. 2000. Ras and Rho GTPases: A family reunion. *Cell.* 103:227–238.
10. Ridley, A. J., and A. Hall. 1994. Signal transduction pathways regulating Rho-mediated stress fibre formation: requirement for a tyrosine kinase. *EMBO J.* 13:2600–2610.
11. Friedl, P. 2004. Dynamic imaging of cellular interactions with extracellular matrix. *Histochem. Cell Biol.* 122:183–190.
12. Hoh, J. H., and C. A. Schoenenberger. 1994. Surface morphology and mechanical properties of MDCK monolayers by atomic force microscopy. *J. Cell Sci.* 107:1105–1114.
13. Zheng, J., P. Lamoureux, V. Santiago, T. Dennerll, R. E. Buxbaum, and S. R. Heidemann. 1991. Tensile regulation of axonal elongation and initiation. *J. Neurosci.* 11:1117–1125.
14. Wang, N., J. P. Butler, and D. E. Ingber. 1993. Mechanotransduction across the cell surface and through the cytoskeleton. *Science.* 260: 1124–1127.
15. Evans, E., K. Ritchie, and R. Merkel. 1995. Sensitive force technique to probe molecular adhesion and structural linkages at biological interfaces. *Biophys. J.* 68:2580–2587.
16. Thoumine, O., and A. Ott. 1997. Time scale dependent viscoelastic and contractile regimes in fibroblasts probed by microplate manipulation. *J. Cell Sci.* 110:2109–2116.
17. Tseng, Y., T. P. Kole, and D. Wirtz. 2002. Micromechanical mapping of live cells by multiple-particle-tracking microrheology. *Biophys. J.* 83:3162–3176.

18. Kole, T. P., Y. Tseng, L. Huang, J. L. Katz, and D. Wirtz. 2004. Rho kinase regulates the intracellular micromechanical response of adherent cells to rho activation. *Mol. Biol. Cell.* 15:3475–3484.

19. Kole, T. P., Y. Tseng, I. Jiang, J. L. Katz, and D. Wirtz. 2005. Intracellular mechanics of migrating fibroblasts. *Mol. Biol. Cell.* 16: 328–338.

20. Xu, J., V. Viasnoff, and D. Wirtz. 1998. Compliance of actin filament networks measured by particle-tracking microrheology and diffusing wave spectroscopy. *Rheologica Acta.* 37:387–398.

21. Tseng, Y., K. M. An, O. Esue, and D. Wirtz. 2004. The bimodal role of filamin in controlling the architecture and mechanics of F-actin networks. *J. Biol. Chem.* 279:1819–1826.

22. Janmey, P. A., S. Hvidt, J. Kas, D. Lerche, A. Maggs, E. Sackmann, M. Schliwa, and T. P. Stossel. 1994. The mechanical properties of actin gels—Elastic modulus and filament motions. *J. Biol. Chem.* 269: 32503–32513.

23. Wachsstock, D., W. H. Schwarz, and T. D. Pollard. 1994. Crosslinker dynamics determine the mechanical properties of actin gels. *Biophys. J.* 66:801–809.

24. Gardel, M. L., M. T. Valentine, J. C. Crocker, A. R. Bausch, and D. A. Weitz. 2003. Microrheology of entangled F-actin solutions. *Phys. Rev. Lett.* 91:158302.

25. Tseng, Y., J. S. Lee, T. P. Kole, I. Jiang, and D. Wirtz. 2004. Micro-organization and visco-elasticity of the interphase nucleus revealed by particle nanotracking. *J. Cell Sci.* 117:2159–2167.

26. Tseng, Y., T. P. Kole, J. S. Lee, E. Fedorov, S. C. Almo, B. W. Schafer, and D. Wirtz. 2005. How actin crosslinking and bundling proteins cooperate to generate an enhanced cell mechanical response. *Biochem. Biophys. Res. Commun.* 334:183–192.

27. Bell, S. E., A. Mavila, R. Salazar, K. J. Bayless, S. Kanagala, S. A. Maxwell, and G. E. Davis. 2001. Differential gene expression during capillary morphogenesis in 3D collagen matrices: regulated expression of genes involved in basement membrane matrix assembly, cell cycle progression, cellular differentiation and G-protein signaling. *J. Cell Sci.* 114:2755–2773.

28. Davis, G. E., K. J. Bayless, and A. Mavila. 2002. Molecular basis of endothelial cell morphogenesis in three-dimensional extracellular matrices. *Anat. Rec.* 268:252–275.

29. Xu, J., D. Wirtz, and T. D. Pollard. 1998. Dynamic cross-linking by α-actinin determines the mechanical properties of actin filament networks. *J. Biol. Chem.* 273:9570–9576.

30. Ghosh, P. K., A. Vasanji, G. Murugesan, S. J. Eppell, L. M. Graham, and P. L. Fox. 2002. Membrane microviscosity regulates endothelial cell motility. *Nat. Cell Biol.* 4:894–900.

31. Byzova, T. V., C. K. Goldman, N. Pampori, K. A. Thomas, A. Bett, S. J. Shattil, and E. F. Plow. 2000. A mechanism for modulation of cellular responses to VEGF: activation of the integrins. *Mol. Cell.* 6:851–860.

32. Gong, C., K. V. Stoletov, and B. I. Terman. 2004. VEGF treatment induces signaling pathways that regulate both actin polymerization and depolymerization. *Angiogenesis.* 7:313–322.

33. van Nieuw Amerongen, G. P., P. Koolwijk, A. Versteilen, and V. W. van Hinsbergh. 2003. Involvement of RhoA/Rho kinase signaling in VEGF-induced endothelial cell migration and angiogenesis in vitro. *Arterioscler. Thromb. Vasc. Biol.* 23:211–217.

34. Kimura, K., M. Ito, M. Amano, K. Chihara, Y. Fukata, M. Nakafuku, B. Yamamori, J. Feng, T. Nakano, K. Okawa, A. Iwamatsu, and K. Kaibuchi. 1996. Regulation of myosin phosphatase by Rho and Rho-associated kinase (Rho-kinase). *Science.* 273:245–248.

35. Wozniak, M. A., R. Desai, P. A. Solski, C. J. Der, and P. J. Keely. 2003. ROCK-generated contractility regulates breast epithelial cell differentiation in response to the physical properties of a three-dimensional collagen matrix. *J. Cell Biol.* 163:583–595.

36. Duguay, D., R. A. Foty, and M. S. Steinberg. 2003. Cadherin-mediated cell adhesion and tissue segregation: qualitative and quantitative determinants. *Dev. Biol.* 253:309–323.

37. Foty, R. A., C. M. Pfleger, G. Forgacs, and M. S. Steinberg. 1996. Surface tensions of embryonic tissues predict their mutual envelopment behavior. *Development.* 122:1611–1620.

38. Suh, J., D. Wirtz, and J. Hanes. 2003. Efficient active transport of gene nanocarriers to the cell nucleus. *Proc. Natl. Acad. Sci. USA.* 100:3878–3882.

39. Lee, J. S., P. Panorchan, C. M. Hale, S. B. Khatau, T. P. Kole, Y. Tseng, and D. Wirtz. 2006. Ballistic intracellular nanorheology reveals ROCK-hard cytoplasmic stiffening response to fluid flow. *J. Cell Sci.* 119:1760–1768.

40. Yamada, S., D. Wirtz, and S. C. Kuo. 2000. Mechanics of living cells measured by laser tracking microrheology. *Biophys. J.* 78:1736–1747.

41. Mason, T. G., K. Ganesan, J. V. van Zanten, D. Wirtz, and S. C. Kuo. 1997. Particle-tracking microrheology of complex fluids. *Phys. Rev. Lett.* 79:3282–3285.

42. Schnurr, B., F. Gittes, F. C. MacKintosh, and C. F. Schmidt. 1997. Determining microscopic viscoelasticity in flexible and semiflexible polymer networks from thermal fluctuations. *Macromolecules.* 30:7781–7792.

43. Tseng, Y., and D. Wirtz. 2001. Mechanics and multiple-particle tracking microheterogeneity of alpha-actinin-cross-linked actin filament networks. *Biophys. J.* 81:1643–1656.

44. Tseng, Y., E. Fedorov, J. M. McCaffery, S. C. Almo, and D. Wirtz. 2001. Micromechanics and microstructure of actin filament networks in the presence of the actin-bundling protein human fascin: A comparison with α-actinin. *J. Mol. Biol.* 310:351–366.

45. Marquez, J. P., G. M. Genin, G. I. Zahalak, and E. L. Elson. 2005. Thin bio-artificial tissues in plane stress: the relationship between cell and tissue strain, and an improved constitutive model. *Biophys. J.* 88:765–777.

46. Zahalak, G. I., J. E. Wagenseil, T. Wakatsuki, and E. L. Elson. 2000. A cell-based constitutive relation for bio-artificial tissues. *Biophys. J.* 79:2369–2381.

47. Wakatsuki, T., M. S. Kolodney, G. I. Zahalak, and E. L. Elson. 2000. Cell mechanics studied by a reconstituted model tissue. *Biophys. J.* 79:2353–2368.

48. Dahl, K. N., S. M. Kahn, K. L. Wilson, and D. E. Discher. 2004. The nuclear envelope lamina network has elasticity and a compressibility limit suggestive of a molecular shock absorber. *J. Cell. Sci.*117:4779–4786.

49. Crisp, M., Q. Liu, K. Roux, J. B. Rattner, C. Shanahan, B. Burke, P. D. Stahl, and D. Hodzic. 2006. Coupling of the nucleus and cytoplasm: role of the LINC complex. *J. Cell Biol.* 172:41–53.

50. Heidemann, S. R., and D. Wirtz. 2004. Towards a regional approach to cell mechanics. *Trends Cell Biol.* 14:160–166.

51. Ridley, A. J., H. F. Paterson, C. L. Johnston, D. Diekmann, and A. Hall. 1992. The small GTP-binding protein Rac regulates growth-factor induced membrane ruffling. *Cell.* 70:401–410.

52. Hall, A., H. F. Paterson, P. Adamson, and A. J. Ridley. 1993. Cellular responses regulated by rho-related small GTP-binding proteins. *Philos. Trans. R. Soc. Lond. B Biol. Sci.* 340:267–271.

53. Svitkina, T. M., and G. G. Borisy. 1998. Correlative light and electron microscopy of the cytoskeleton of cultured cells. *Methods Enzymol.* 298:570–592.

54. Rousseau, S., F. Houle, H. Kotanides, L. Witte, J. Waltenberger, J. Landry, and J. Huot. 2000. Vascular endothelial growth factor (VEGF)-driven actin-based motility is mediated by VEGFR2 and requires concerted activation of stress-activated protein kinase 2 (SAPK2/p38) and geldanamycin-sensitive phosphorylation of focal adhesion kinase. *J. Biol. Chem.* 275:10661–10672.

55. Somlyo, A. V., C. Phelps, C. Dipierro, M. Eto, P. Read, M. Barrett, J. J. Gibson, M. C. Burnitz, C. Myers, and A. P. Somlyo. 2003. Rho kinase and matrix metalloproteinase inhibitors cooperate to inhibit angiogenesis and growth of human prostate cancer xenotransplants. *FASEB J.* 17:223–234.

56. Condeelis, J., and J. E. Segall. 2003. Intravital imaging of cell movement in tumours. *Nat. Rev. Cancer.* 3:921–930.

57. Helmke, B. P. 2005. Molecular control of cytoskeletal mechanics by hemodynamic forces. *Physiology (Bethesda).* 20:43–53.